Aspect Ratio Plays a Role in the Hazard Potential of CeO_2 Nanoparticles in Mouse Lung and Zebrafish Gastrointestinal Tract

Sijie Lin,[†,#] Xiang Wang,[†,#] Zhaoxia Ji,[†,#] Chong Hyun Chang,[†] Yuan Dong,[‡] Huan Meng,[†,§] Yu-Pei Liao,[§] Meiying Wang,[§] Tze-Bin Song,[∥] Sirus Kohan,[⊥] Tian Xia,[†,§] Jeffrey I. Zink,[⊗] Shuo Lin,[‡] and André E. Nel[†,§,*]

[†]Center for Environmental Implications of Nanotechnology, California NanoSystems Institute, [‡]Department of Molecular, Cell and Developmental Biology, [§]Division of NanoMedicine, Department of Medicine, [∥]Department of Materials Science and Engineering, [⊥]Brain Research Institute, and [⊗]Department of Chemistry and Biochemistry, University of California, Los Angeles, California 90095, United States. [#]S. Lin, X. Wang, and Z. Ji contributed equally.

ABSTRACT We have previously demonstrated that there is a relationship between the aspect ratio (AR) of CeO_2 nanoparticles and *in vitro* hazard potential. CeO_2 nanorods with AR ≥ 22 induced lysosomal damage and progressive effects on IL-1β production and cytotoxicity in the human myeloid cell line, THP-1. In order to determine whether this toxicological paradigm for long aspect ratio (LAR) CeO_2 is also relevant *in vivo*, we performed comparative studies in the mouse lung and gastrointestinal tract (GIT) of zebrafish larvae. Although oropharyngeal aspiration could induce acute lung inflammation for CeO_2 nanospheres and nanorods, only the nanorods with the highest AR (C5) induced significant IL-1β and TGF-β1 production in the bronchoalveolar lavage fluid at 21 days but did not induce pulmonary fibrosis. However, after a longer duration (44 days) exposure to 4 mg/kg of the C5 nanorods, more collagen production was seen with CeO_2 nanorods *vs* nanospheres after correcting for Ce lung burden. Using an oral-exposure model in zebrafish larvae, we demonstrated that C5 nanorods also induced significant growth inhibition, a decrease in body weight, and delayed vertebral calcification. In contrast, CeO_2 nanospheres and shorter nanorods had no effect. Histological and transmission electron microscopy analyses showed that the key injury mechanism of C5 was in the epithelial lining of the GIT, which demonstrated blunted microvilli and compromised digestive function. All considered, these data demonstrate that, similar to cellular studies, LAR CeO_2 nanorods exhibit more toxicity in the lung and GIT, which could be relevant to inhalation and environmental hazard potential.

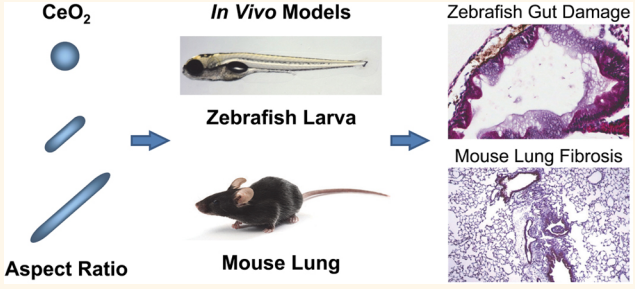

KEYWORDS: CeO_2 nanoparticle · long aspect ratio · hazard potential · mouse lung · zebrafish gastrointestinal tract

Long aspect ratio (LAR) nanomaterials are increasingly being used in semiconductors, catalysts, microelectromechanical systems, food packaging, and biomedicine because of the acquisition of unique physicochemical properties.[1−5] Because increased industrial use also raises the chances of human and environmental exposure, we have recently constructed a CeO_2 nanoparticle library in which the AR of the nanoparticles ranged from 1 (nanospheres) to >100 (nanorods).[6] CeO_2 is important because of its widespread use in fuel additives, polishing materials, energy production, and biomedical applications.[7,8] In addition, more attention is paid to one-dimensional CeO_2 nanostructures such as nanorods, nanowires, and nanotubes due to their high redox and catalytic activities. In a recent study, synthesis of CeO_2 nanoparticles with various shapes (nanopolyhedra, nanorods, and nanocubes) has demonstrated that nanorods exhibited the highest oxygen-storage capacity.[9] In another study, Zhou *et al.* showed the superior reduction capabilities of CeO_2 nanotubes compared to the conventional nanoparticles.[10] Using a human myeloid cell line, THP-1, we showed that CeO_2 nanorods with an AR ≥ 22 can induce a progressive increase in IL-1β production by generating lysosomal damage and assembly of the NLRP3 inflammasome.[6]

* Address correspondence to anel@mednet.ucla.edu.

Received for review December 16, 2013 and accepted April 10, 2014.

Published online April 10, 2014
10.1021/nn5012754

By contrast, CeO_2 nanospheres and shorter nanorods did not show any significant toxicity. A key question therefore becomes whether the AR of CeO_2 could also impact this material's *in vivo* hazard potential. An important target organ is the lung, because of the dispersive nature of these materials, including a recent demonstration that CeO_2 nanoparticles exhibit the potential to induce pulmonary fibrosis.[7,11] Moreover, it is also important to consider the environmental impact of LAR materials, toward which we use zebrafish embryos and larvae as a model for studying the toxicity of oxide nanoparticles.[12−14]

The rodent lung is frequently used to assess the hazard potential of respirable engineered nanomaterials (ENM), including LAR materials such as TiO_2 nanobelts, single-wall (SWNT) and multiwall carbon nanotubes (MWCNTs).[15−19] Collectively, these studies show that LAR materials are capable of inducing acute neutrophilic as well as subchronic granulomatous inflammation, leading to pulmonary fibrosis.[18−20] One of the mechanisms by which LAR materials induce subchronic lung injury is triggering of frustrated phagocytosis in macrophages, which may fail to digest biopersistent fibers more than 15 μm in length.[21] At this length scale, materials such as asbestos fibers are capable of piercing the surface membrane of the phagocyte, leading to leakage of highly inflammatory hydrolytic enzymes and reactive oxygen species (ROS), which result in chronic lung injury and fibrosis.[21−23] However, most CeO_2 nanorods do not fall into the fiber length scale, and it is important to consider other injury mechanisms in pulmonary macrophages, including lysosomal injury by LAR materials in the nanometer to the lower micrometer length scale.[6,18,24−26] Lysosomal injury results in the assembly of the NRLP3 inflammasome, which leads to IL-1β release by pulmonary macrophages; this cytokine may then initiate a progressive cascade that culminates in pulmonary fibrosis.[18,24−26] The particle dose, subcellular localization, and rate of clearance of the LAR materials from the lung establish lung burden that, during CeO_2 nanoparticle overload, could determine whether an exposure will result in chronic injury.[20,21,23] To date there has been no systematic dissection of the role of CeO_2 AR and shape in the events that may contribute to chronic or subchronic lung injury.

Although limited environmental studies showed that CeO_2 nanoparticles induce toxic effects in green algae and cyanobacteria,[27,28] no systematic toxicological analyses have been undertaken to assess the role of AR in environmental organisms. While it has been demonstrated that a LAR material such as CNTs can exert hazardous effects in daphnia, zebrafish, and rainbow trout, these outcomes have been attributed to the hydrophobicity, state of agglomeration, and heavy metal content rather than AR.[29−32] Interestingly, while SWCNTs can induce severe respiratory toxicity in fish due to gill damage,[31] it has been demonstrated that dendritic nickel nanoparticles can cause injury due to a shape effect in the gastrointestinal tract (GIT) of zebrafish larvae.[33] This injury, as a result of interference in epithelial folding and thinning of intestinal wall, was observed only during exposure to dendritic particles, but was not seen with spheres or nickel ions. Moreover, Gilbert *et al*. have recently shown that daphnia ingesting Ag nanowires display a distinct pattern of gene expression compared to the ones exposed to ionic Ag.[34] These results suggest that nanoparticle shape could play a role in GIT toxicity.

The objective of this study was to perform a comparative analysis of the effects of spherical and rod-shaped CeO_2 nanoparticles in the mouse lung and the GIT of zebrafish larvae. After the synthesis and characterization of a fresh library of CeO_2 nanospheres and nanorods, the biological impact of AR was confirmed in bone marrow macrophages before embarking on *in vivo* studies. Oropharyngeal aspiration of nanospheres and nanorods was performed in C57BL/6 mice to compare their ability to generate acute and subchronic inflammation in the lung. While all the CeO_2 nanoparticles could induce acute neutrophil inflammation in the lung, there was no significant correlation to AR, except that the longest nanorods (C5) could induce more IL-1β production than other materials. While all the materials could induce pulmonary fibrosis after 44 days, the longest rod (C5) induced more collagen deposition after correcting for lung burden. Oral exposure of zebrafish larvae to C5 nanorods also induced significant damage to the microvilli of the GIT epithelial cells. This led to digestive malfunction, which interfered in the growth and development of exposed larvae. These results are important in considering the potential toxicity of CeO_2 in occupational and environmental exposures.

RESULTS

Establishing a CeO_2 Aspect Ratio Library with Differential Toxicological Effects. Using hydrothermal synthesis, we prepared a library of CeO_2 nanoparticles that included nanospheres (AR = 1, C1) and nanorods showing ARs of 8 (C2), 22 (C3), 52 (C4), and >100 (C5) (Figure 1). The size, shape, and AR of CeO_2 were characterized in their dry state using transmission electron microscopy (TEM), while the hydrodynamic diameter and surface charge were measured in deionized water, tissue culture medium (DMEM supplemented with 10% FBS), and zebrafish growth medium (Holtfreter's buffer, supplemented with 100 ug/mL alginate). Figure 1 shows the representative TEM images of C1−C5. As shown in the included table, the average diameters of the nanorods were 7−10 nm, while the average lengths ranged from 50 nm to >1 μm. When dispersed in the tissue culture and Holtfreter's media, the hydrodynamic diameters of the CeO_2 nanoparticles ranged

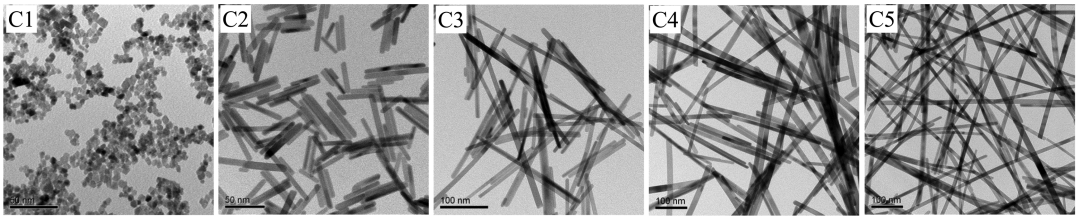

Sample name	L (nm)	D (nm)	AR	Hydrodynamic diameter (nm) DI H_2O	DMEM	Holtfreter's medium	zeta-potential (mV) DI H_2O	DMEM	Holtfreter's medium
C1	N/A	7	1	56 ± 1	223 ± 3	805 ± 38	40.6 ± 2.2	-11.3 ± 3.0	-32.4 ± 1.4
C2	50.8	6.7	8	265 ± 3	444 ± 37	782 ± 48	38.2 ± 2.4	-11.1 ± 2.6	-31.6 ± 2.8
C3	197.2	9.1	22	449± 27	705 ± 59	1001 ± 23	31.6 ± 1.1	-11.1 ± 1.8	-19.72 ± 2.6
C4	495.7	9.5	52	643 ± 109	1382 ± 59	719 ± 10	32.7 ± 2.0	-15.3 ± 1.3	-24.92 ± 2.2
C5	>1000	9.5	>100	900 ± 41	1570 ± 238	1248 ± 71	11.7 ± 0.6	-10.4 ± 1.6	-32.55 ± 1.8

Figure 1. Physicochemical characterization of CeO_2 nanospheres and nanorods. (A) Representative TEM images show the primary size, shape, and AR of CeO_2 (C1, C2, C3, C4, and C5). (B) Table summarizing the diameter, length, and AR of CeO_2 based on the TEM analysis, as well as the hydrodynamic diameter and surface charge of nanoparticles suspended in distilled water, cell culture medium (DMEM), and zebrafish growth medium (Holtfreter's medium).

from 200 nm to 1.5 μm. It should be noted that the hydrodynamic diameters reported here for the CeO_2 nanorods represent only "relative" size and cannot be used to infer exact particle size. Nonetheless, our studies on CNTs demonstrate the utility of the DLS measurement as a qualitative index of the state of dispersal of long aspect ratio materials.[6,25,26] While the zeta potentials of the CeO_2 nanoparticles were in the range of 10 to 40 mV in distilled water, the surface charge became negative (−10 to −30 mV) upon coating with FBS or alginate.

In order to confirm the biological impact of AR variation, we used the myeloid cell line, THP-1, and bone marrow derived macrophages (BMDM) to determine whether the nanospheres and nanorods differ in their ability to initiate IL-1β production. We have previously shown that IL-1β release from myeloid cells and macrophages is determined by the impact of AR on the lysosome.[25,26] As shown in Figure S1A and B, cellular incubation with CeO_2 nanospheres and nanorods resulted in a progressive increase in IL-1β production in accordance with the AR. The effects of the CeO_2 nanorods became statistically significant above AR of 22. We confirmed that this effect involves lysosome activation and NLRP3 inflammasome assembly (not shown).[6]

Acute Pulmonary Exposure to CeO_2 Nanospheres and Nanorods. C57BL/6 mice were used for exposure to 0.5, 1, 2, and 4 mg/kg of the C5 nanorods by oropharyngeal aspiration. The mice were sacrificed after 40 h to collect bronchoalveolar lavage fluid (BALF) and lung tissue. Aspiration of Min-U-Sil (quartz, or QTZ) was used as positive control. Examination of the BALF showed a dose-dependent increase in the neutrophil cell count, along with an increase in LIX (LPS-induced CXC chemokine), which is involved in neutrophil chemotaxis (Figure 2A,B). We also observed an increase in IL-1β production, which may constitute the early phase of a delayed injury response for some LAR materials (Figure 2C).[24−26] QTZ also induced increased IL-1β production. On the basis of the dose response data for C5 nanorods, we selected 2 mg/kg for comparative analysis of C1, C2, C3, and C5 in further lung exposure studies.

In a comparative study in which animal sacrifice was performed after 40 h, all the nanoparticles could induce an increase in neutrophil cell counts, with a tendency for the acute inflammatory response to be higher for the LAR materials. The neutrophil cell counts for C5 ($(3.2 \pm 0.7) \times 10^4$/mL) was significantly higher than for C1 ($(2.0 \pm 0.5) \times 10^4$/mL) (Figure 3A). However, this effect was accompanied by a nonselective but statistically significant increase in LIX levels for all particles tested (Figure 3B). The trend toward more inflammation by C5 was confirmed by H&E staining, which showed visual evidence of more acute inflammatory infiltrates around small- and medium-sized airways in the lung of animals receiving the LAR particles (Figure S2). Again, the effect of the C5 nanorods was most pronounced (Figure S2). QTZ also induced significant increases in neutrophil counts and LIX levels in the BALF along with inflammatory changes in the lung (Figure 3A,B, and Figure S2). In contrast, the data for IL-1β production was quite different in that only C5 and QTZ induced significant increases in the BALF (Figure 3C). This suggested to us that, similar to the C5 dose response study, it would be important to address possible delayed injury.

C5 Nanorods Show an Exaggerated Pro-fibrogenic Response after Subchronic Exposure. In order to determine whether the observed IL-1β production at 40 h is indicative of subchronic lung injury, we performed a study in which the animal sacrifice was performed 21 days after

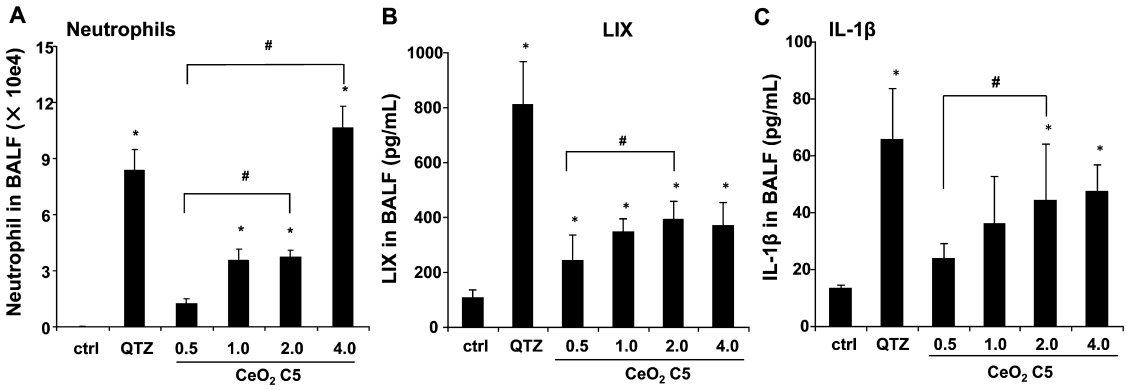

Figure 2. Acute pulmonary effects of CeO_2 nanoparticles in C57BL/6 mice. The dose-dependent experiment was carried out in mice exposed to CeO_2 nanoparticles C5 at 0.5, 1.0, 2.0, and 4.0 mg/kg by oropharyngeal aspiration. There were 6 animals per group. Animals were euthanized after 40 h, and BALF was collected to determine neutrophil cell counts (A), LIX (B), and IL-1β (C) levels. Animals exposed to 5.0 mg/kg QTZ were used as positive control. The experiment was reproduced a second time; $^*p < 0.05$ compared to control; $^\#p < 0.05$ for pairwise comparisons as shown.

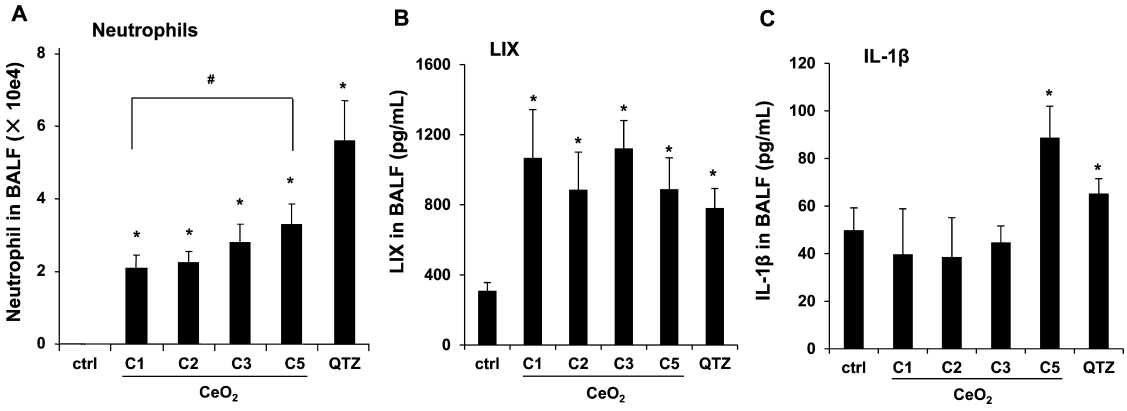

Figure 3. Acute pulmonary effects of CeO_2 nanoparticles in mice. The comparison experiment was carried out in C57BL/6 mice exposed to CeO_2 nanoparticles C1, C2, C3, and C5 at 2.0 mg/kg by oropharyngeal aspiration. There were 6 animals per group. Mice were sacrificed at 40 h, and the neutrophil cell counts (A), LIX (B), and IL-1β (C) levels in BALF were determined. QTZ at 5.0 mg/kg was used as a positive control. The experiment was reproduced a second time; $^*p < 0.05$ compared to control; $^\#p < 0.05$ for pairwise comparisons as shown.

oropharyngeal instillation of C1, C3, and C5 at 2 mg/kg. No evidence of neutrophil infiltration was obtained at this point (data not shown). While IL-1β levels also returned to baseline (not shown), measurement of TGF-β1 levels in the BALF showed that C5 induced a significant increase in TGF-β1 production, while C1 and C3 failed to induce a response (Figure 4A). However, none of the materials induced collagen deposition, as determined by a Sircol assay (Figure 4B) or Masson's trichrome staining of the lung sections (Figure S3). In contrast, QTZ induced a significant TGF-β1 production and collagen deposition (Figure 4A,B and S3). Because collagen deposition by TiO_2 nanobelts was seen to occur after several months,[19] a third series of experiments were undertaken in which sacrifice was performed 44 days after oropharyngeal aspiration of 4 mg/kg. In this scenario, clear evidence was obtained of increased TGF-β1 production in the BALF (Figure 5A), along with increased collagen content in lung tissue (Figure 5B) and positive (blue color) trichrome staining (Figure 5C) for all tested materials, including QTZ. However, since ENMs with different ARs may have different rates of retention and bioavailability, we used inductively coupled plasma optical emission spectrometry (ICP-OES) to determine the total lung burden for Ce in C1- and C5-exposed animals. This demonstrated that there was indeed a significant difference in the lung burden of nanospheres and nanorods (Figure 5D). That is, the total Ce content in the lung of C1-exposed animals was six times higher than C5, suggesting a higher clearance rate and/or lower bioavailability for C5 compared to C1. Use of the Ce content to adjust the collagen content in the lung (*i.e.*, expressing collagen content per unit mass of Ce) demonstrated that there was indeed more collagen deposition per unit dose of C5 (Figure 5E). These data indicate that while all CeO_2 nanoparticles induce pulmonary fibrosis at a dose of 4 mg/kg, the response is strongest for C5, showing that AR could play a role in subchronic lung injury.

AR Plays a Role in Growth Inhibition and Development of Zebrafish Larvae. We developed a pulse-exposure method

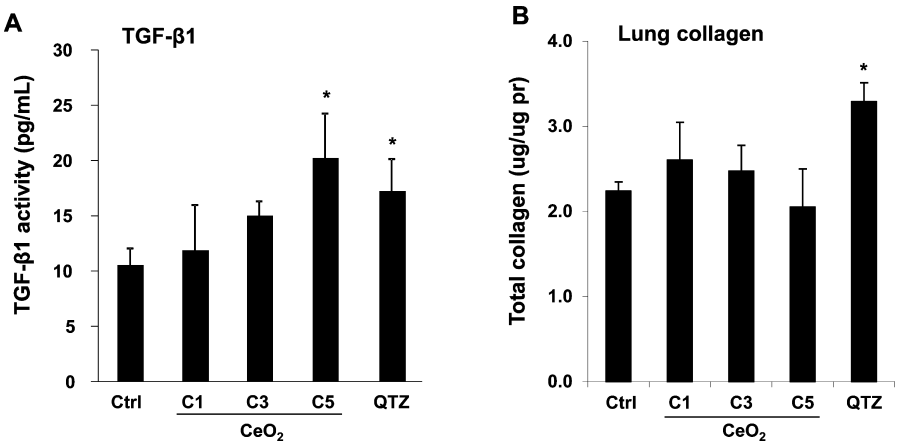

Figure 4. Subchronic pulmonary effects of CeO_2 nanoparticles at 21 days. The experiment was performed as in Figure 3, except that the mice were sacrificed 21 days after the oropharyngeal aspiration. BALF was collected to determine the TGF-β1 (A) level. (B) The total collagen content of the lung tissues was determined by the Sircol collagen kit (Biocolor Ltd., Carrickfergus, U.K.). QTZ at 5.0 mg/kg was treated as a positive control. *$p < 0.05$ compared to control.

for zebrafish larvae in Petri dishes to limit the amount of CeO_2 nanoparticles that would be required for exposures in standard aquarium tanks. Petri dish exposure also limits the amount of hazardous waste being generated. The exposure sequence is summarized in Figure 6A and discussed in detail in the Materials and Methods. Briefly, groups of 30 larvae 5 days postfertilization (dpf) were incubated with 25 μg/mL C1, C3, C4, and C5 nanoparticles in each Petri dish for 6 h. The larvae were carefully and thoroughly washed before returning them to 3 L aquarium tanks for regular maintenance. Second and third round pulse-exposures were carried out on the same larvae at 8 and 11 dpf, respectively. Citrate-coated silver nanoparticles (AgNPs) of 20 nm were used as a positive control.[35−37] The larvae were assessed for overall health status, survival rate, gross morphological abnormalities, body length, weight, and number of calcified vertebrae (as a biomarker of skeletal development). While no significant mortality was observed for any of the CeO_2 nanomaterials (Figure 6B), the larval length was significantly reduced by C4 and C5 exposures at 14 dpf compared to larvae exposed to C1 and C3 (Figure S4). While the larval morphology was grossly normal, the absence of dorsal and anal fin structures in the C4- and C5-exposed larvae suggested delayed development. In contrast, the larvae exposed to AgNPs showed a decreased survival rate, smaller size, and higher rate of morphological abnormalities (*e.g.*, the bent spine depicted in Figure S4). Quantitative expression of the measurements of larval length and weight also confirmed that C5-exposed animals had significant growth retardation compared to the control or C1/C3-exposed animals (Figure 6C and D). The same was true for AgNP exposure. Since calcification of skeletal structures occurs in a caudal-to-rostral fashion, vertebral calcification is also a good parameter to assess larval development.[38] Calcification can be assessed by the green fluorescent chromophore calcein, which is taken up and allows visualization of the calcified vertebrae. Quantification of the number of calcified vertebrae showed that larvae exposed to C5 (and AgNPs) had significantly fewer calcified vertebral segments by 14 dpf (Figure 6E). Taken together, both qualitative and quantitative assays demonstrate an AR threshold, above which CeO_2 nanorods induce growth inhibition and abnormal development. This raises the question of the site(s) of injury by LAR materials in larvae.

Assessment of CeO_2 Nanoparticle Uptake in the GIT of Zebrafish Larvae. In order to study CeO_2 bioavailability, leading to interference in larval growth and development, we initially used light optical microscopy to look for the presence of the nanoparticles in the zebrafish larvae. This demonstrated the presence of CeO_2 aggregates in the GIT lumen of larvae at 120 hpf (Figure 7A, left panel). The presence of CeO_2 was confirmed by a signature CeO_2 Raman peak, using confocal Raman microscopy (Figure 7A, right panel).[39,40] Raman spectra collected from the skin, fins, or blood vessels did not show the presence of CeO_2, suggesting the GIT is a major target organ. This notion was strengthened by the lack of any CeO_2 uptake in the GIT of 72 hpf embryos, which lacks a mouth opening for feeding (not shown). In contrast, 120 hpf larvae do express a mouth opening (Figure 7B).

Further studies were carried out to assess the amount of CeO_2 uptake by ICP-OES (Figure 7B). Assessment of the Ce content in 120 dpf larvae exposed to C1 and C5 nanoparticles demonstrated that, immediately following larval exposure for 6 h, the animals exposed to C1 contained 14.52 μg Ce per g of larval body weight, while those exposed to C5 contained 14.34 μg Ce per g of larval body weight. Repeat of the ICP-OES analysis in 144 hpf larvae, 24 h after a 6 h exposure, showed a steep decline in both C1 and C5 Ce content, suggesting that most of the material was cleared from the GIT. This was also confirmed by light

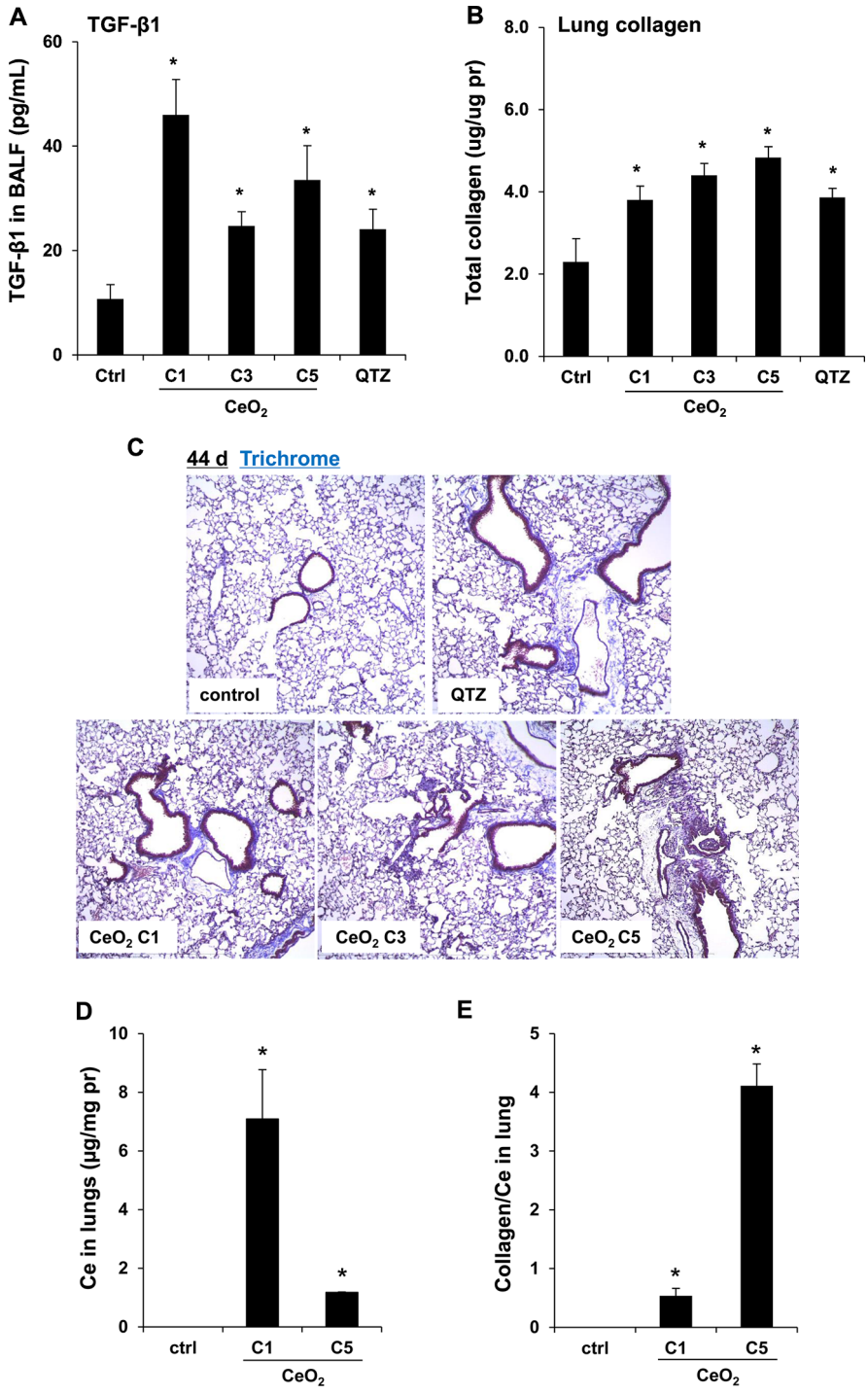

Figure 5. Subchronic pulmonary effects of CeO_2 nanoparticles at 44 days. (A) TGF-β1 levels in BALF and (B) total collagen content of the lungs of mice receiving 4 mg/kg CeO_2 nanoparticles. The animals were sacrificed after 44 days, and all lung tissues were collected to determine the total collagen as described in Figure 4. (C) Lung sectioning and staining with Masson's trichrome. Areas of concentrated blue staining represent collagen deposition sites. QTZ at 5.0 mg/kg served as a positive control. (D) ICP-OES analysis to determine elemental Ce content in the lungs of mice receiving the same dose of C1 and C5 nanoparticles, followed by sacrifice after 44 days. (E) Comparative analysis of the collagen content in the lung of C1- and C5-exposed mice after correction for Ce content. This was accomplished by normalizing the total collagen content to the total elemental Ce content and expressed as collagen/Ce in lung. *$p < 0.05$ compared to control.

optical microscopy. TEM analysis of the pseudofeces collected at the bottom of the aquarium tanks confirmed the presence of CeO_2 agglomerates (Figure S5). In accordance with the requirement of GIT uptake by the mouth, embryos lacking an oral aperture (24 and 72 hpf) had no discernible Ce uptake.

Assessment of GIT Damage by LAR CeO_2 Nanoparticles. Since the GIT is the main target organ for CeO_2

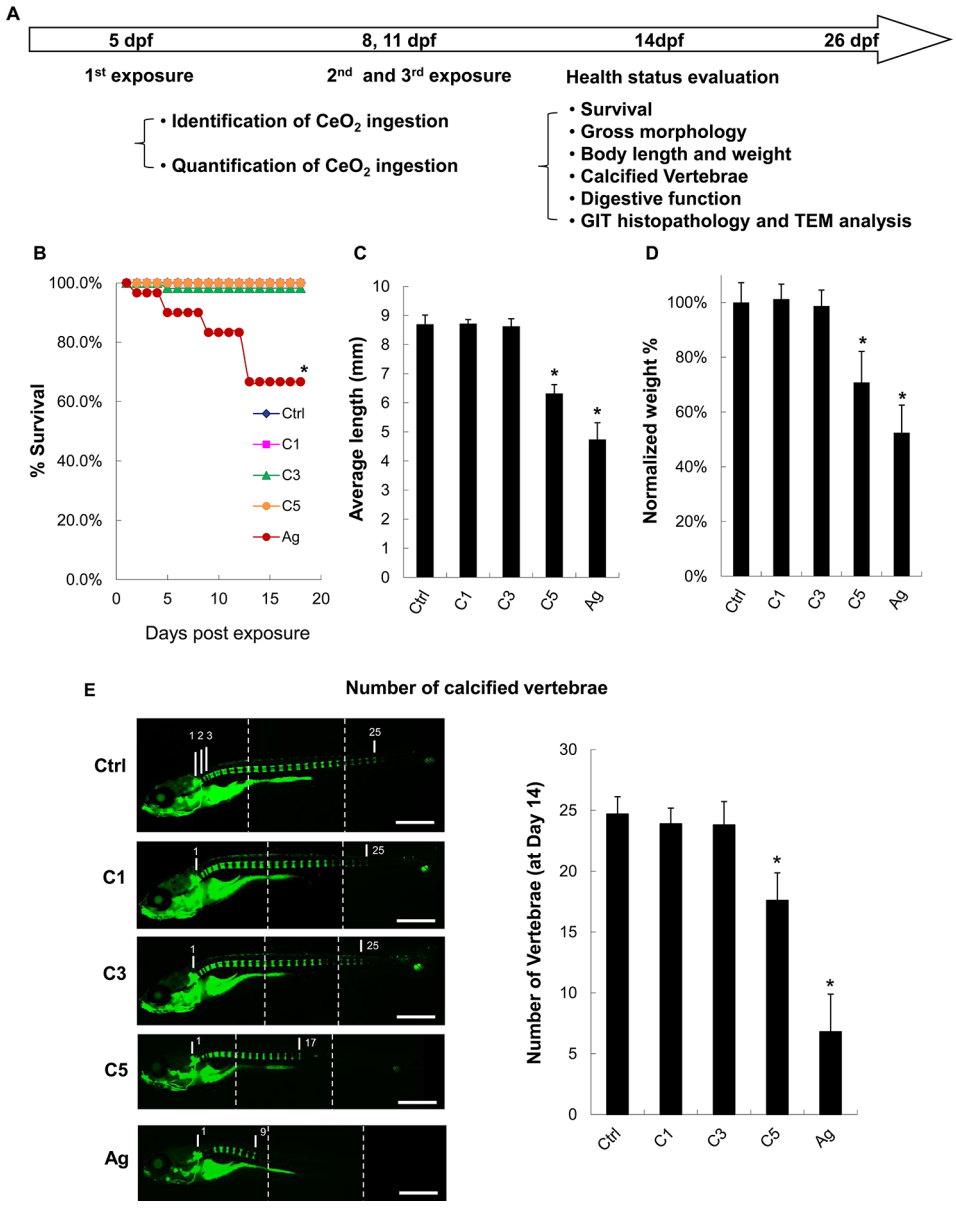

Figure 6. Pulse-exposure of zebrafish larvae to CeO_2 nanoparticles to assess the effect of AR on larval development. (A) Diagram showing the stepwise pulse-exposure protocol. Zebrafish larvae at 5 dpf were incubated in CeO_2 nanoparticle suspensions in Petri dishes. Thirty larvae were exposed on each occasion to 25 μg/mL nanoparticles for 6 h. The larvae were carefully and thoroughly washed before returning to standard aquarium tanks for regular feeding and water circulation. The same batch of larvae was used for secondary and tertiary exposures at 8 and 11 dpf. The survival rate of larvae was monitored daily, and the overall health status of the larvae assessed on 14 dpf based on morphology features, body length and weight, number of calcified vertebrae, and digestive function. Larvae were also randomly selected for histology and TEM analyses. (B) Survival rate of untreated larvae or larvae exposed to C1, C3, C5, and AgNPs. Only the larvae exposed to AgNPs (positive control) showed decreased survival. (C) Average larval length at 14 dpf. Larvae exposed to C5 and AgNPs showed a significantly reduced length. (D) Average larval weight showed that C5 and AgNP exposures resulted in significantly lower body weight. (E) Use of the number of calcified vertebrae as assessed by calcein staining. The representative fluorescence images show that control or larvae exposed to C1 and C3 exhibit 25 calcified vertebrae at 14 dpf. By contrast, larvae exposed to C5 and AgNPs showed ~17 and ~9 calcified vertebrae, respectively. Three images were captured and blended to cover the total body length, as indicated by the dashed lines. *$p < 0.05$ compared to control. Scale bar: 1 mm.

nanoparticles at the larval stage, histological and TEM analyses were performed in zebrafish exposed to C1 and C5 nanoparticles 3 days after the third pulse-exposure (*i.e.*, 14 dpf). H&E staining revealed clear evidence of structural damage by C5 but not C1. Specifically, C5 ingestion was associated with desquamation of the enterocytes and development of a vacuolar appearance in the intestinal lining (Figure 8A). TEM analysis of a GIT section confirmed the presence of C5-associated ultrastructural damage, which showed up as blunting of microvilli and epithelial atrophy (Figure 8B). Bundles of the LAR nanoparticles could be seen to pierce and disrupt the structure of microvilli (Figure 8C, Figure S6A and B). However, in spite of this

damage, C5 nanorods could not be seen to be directly taken up into epithelial cells or gain access to subepithelial tissue. Instead, the C5 nanorods passed through the GIT and appeared in the pseudofeces (Figure S5A and B). In contrast, C1 was not associated with any damage to the closely stacked microvilli, in spite of nanoparticle adherence to the tips of the microvilli (Figure 8C).

In order to reconcile the structural GIT damage with the developmental abnormalities depicted in Figures 6B–E, we asked whether this was due to interference in digestive function. In order to test digestive function, we used an *in vivo* fluorescence-based technique to monitor the digestion of an intramolecular-quenched protein (EnzChek).[41,42] EnzChek was fed to the larvae a day after exposure to CeO_2 nanoparticles. Digestion of this protein releases fluorescent peptides, which can be quantitatively assessed by fluorescence spectroscopy (Figure 9A) or the use of ImageJ software that analyzes fluorescence microscopy images in intact larvae (Figure 9B, left panel). Scoring of the fluorescence intensity by ImageJ analysis demonstrated that C5, but not C1 or C3, could induce a decrease in fluorescence intensity in the GIT of exposed larvae (Figure 9B, right panel). This confirms that C5 nanorods can induce GIT damage, leading to digestive malfunction and developmental abnormalities.

DISCUSSION

In this study, we compared the *in vivo* effects of LAR CeO_2 nanoparticles with nanospheres in the murine lung as well as zebrafish intestinal tract. The oropharyngeal aspiration studies in the mice showed that at a dose of 4 mg/kg all CeO_2 nanoparticles induced fibrogenic effects in the lung, culminating in pulmonary fibrosis 44 days later. However, if corrected for the higher lung burden of the nanospheres, the material with the longest AR material (C5) induced more fibrosis than the spheres (C1). The ability of LAR CeO_2 (C5) to induce IL-1β and TGF-β1 production in the lung at supra-threshold amounts may play a role in the fibrogenic effects of these materials. This agrees with the structure–activity relationship (SAR) analysis in THP-1 cells and BMDMs, where LAR injury is accompanied by NLRP3 assembly and IL-1β production. C5 nanorods also resulted in prominent injury to the GIT of zebrafish larvae, while shorter rods or spherical nanoparticles had no effect. The mechanistic basis of this injury appears to be the ability of C5 to damage the microvilli, resulting in digestive malfunction, nutritional deficiency, retarded growth, and abnormal physical development. Interestingly, the C5 nanorods did not differ from the nanospheres with respect to nanoparticle uptake and retention kinetics in the GIT. All considered, these results demonstrate the importance of CeO_2 AR in occupational and environmental hazard assessment.

The pulmonary hazard potential of CeO_2 is an important consideration based on the dispersive nature of these materials, which are being used as additives for fossil fuel combustion, polishing of material surfaces, and biomedical devices.[11,43] Mining of rare earth metals, of which cerium is a major ingredient (80%), has also been reported to be associated with an occupational pneumoconiosis, characterized by granulomatous inflammation and interstitial fibrosis.[44,45] Moreover, tracheal instillation studies in rats have shown that spherical CeO_2 nanoparticles can induce lung fibrosis in a dose- and time-dependent manner.[7,11,44,45] While the mechanism(s) of the pro-fibrogenic effects is/are uncertain, it has been suggested that CeO_2 particles generate ROS and oxidative stress that could be involved in lung injury.[7,46,47] However, compared to a list of more toxic metal oxide nanoparticles, we have found CeO_2 to be relatively inert in terms of oxidant injury in the lung, in addition to literature reporting CeO_2's antioxidant effects as a result of difference in valence state.[7,48–50] Another biological injury could occur due to the high binding affinity of rare earth oxides for cellular phosphate groups, including membrane phospholipids and cellular phosphoproteins.[51] However, CeO_2 did not exhibit a strong effect in this regard compared to the effect of other rare earth oxides.[51] Similar to the studies of the pro-fibrogenic potential of CeO_2 in the rat lung,[11] collagen deposition in the mouse lung was accompanied by TGF-β1 production. TGF-β1 is a pro-fibrogenic growth factor that is produced as a component of a lung fibrosis cascade that commences during an early stage as IL-1β production in activated pulmonary macrophages. Activated macrophages cooperate with pulmonary epithelial cells, which transition to mesenchymal cells and fibroblasts depositing collagen in the lung.[25,26,52] Our previous study and this article indicate that the AR of the CeO_2 nanoparticles plays a role in these trophic cellular interactions by triggering a pathway that involves lysosomal damage and NLRP3 inflammasome activation.[6] Moreover, we have previously demonstrated that there is a specific threshold above which the AR triggers lysosomal damage and NLRP3 assembly, as confirmed by the data in Figure S1A and B. Pertaining to the particles used in this study, it is interesting that the length of the C5 stacking bundles (0.75 to 2 μm) exceeds the lysosomal diameter, which varies from ~1.1 to 2.9 μm.[6,53] We propose, therefore, that above a dose of 2 mg/kg, LAR dimension contributes to IL-1β production and determines the extent of pulmonary fibrosis. It is interesting that the CeO_2 nanospheres are better retained in the lung than C5 nanorods and that the AR contribution could be seen to emerge only if the collagen content is corrected for Ce lung burden (Figure 5E). The higher lung burden of the spheres could be due to more lung uptake, but could also result from lower bioavailability and/or higher clearance rate of C5.[23,54] Another unique accomplishment of this work was the

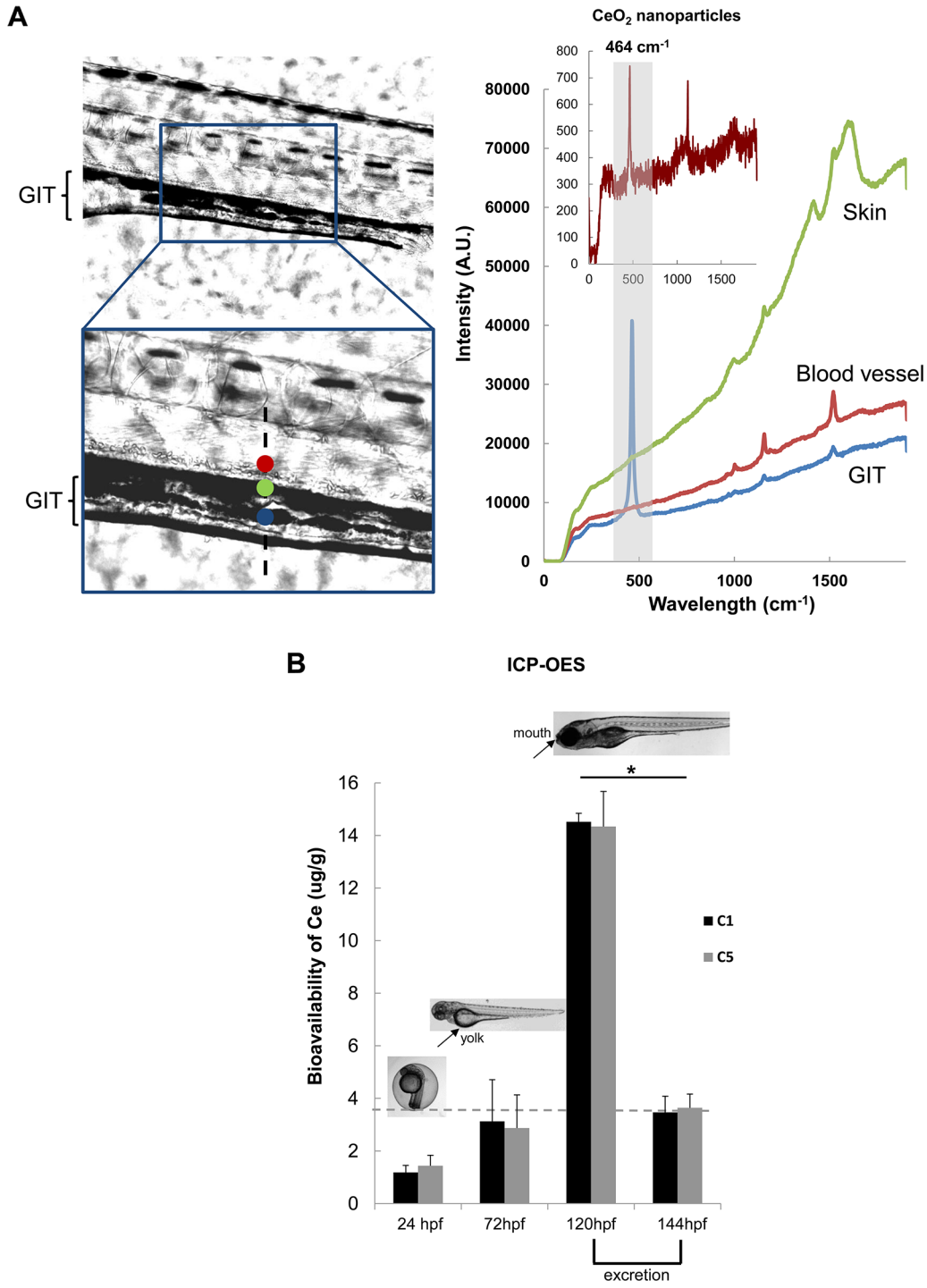

Figure 7. Confocal-Raman microscopy and ICP-OES analyses of CeO_2 uptake in zebrafish embryos and larvae after nanoparticle exposure. (A) Confocal Raman microscopy analysis was conducted on the C5-exposed larvae. The signature Raman scattering peak of CeO_2 (centered at 464 cm^{-1}) confirmed the presence of C5 inside the GIT. Raman spectra collected from the skin (green dot) or the blood vessels (red dot) did not show any signature peak for CeO_2. Developing larvae were anesthetized and placed on a glass slide with concavity wells. The excitation laser beam (514 nm) was programmed to scan across the lateral view of developing larvae as indicated by the dashed line. Raman scattering spectra were collected across this line at three spots (red dot = skin, green = blood vessel, blue = GIT). Among these, only the blue spot showed a Raman signature similar to that of CeO_2 nanoparticles (provided in the inset). (B) Groups (n = 50) of embryos (24 and 72 hpf) and larvae (120 hpf) were incubated with 25 μg/mL CeO_2 (C1 and C5) for 6 h. The embryos and larvae were thoroughly washed before acid digestion and assessment of the amount (μg) of Ce by ICP-OES. The elemental Ce content in 24 and 72 hpf embryos was 1.5−3.0 μg/g of embryos, which is close to the detection limit of ICP-OES (indicated by gray dash line). This quantity went up to 14.52 and 14.34 μg/g of larvae exposed to C1 and C5, respectively, if the exposure was performed at 120 hpf. However, incubation of these larvae for an additional 24 h (*i.e.*, up to 144 hpf) showed a significant reduction in the Ce content upon elimination from the gut (*$p < 0.05$). There was no statistically significant difference between uptake of C1 and C5 at any time point.

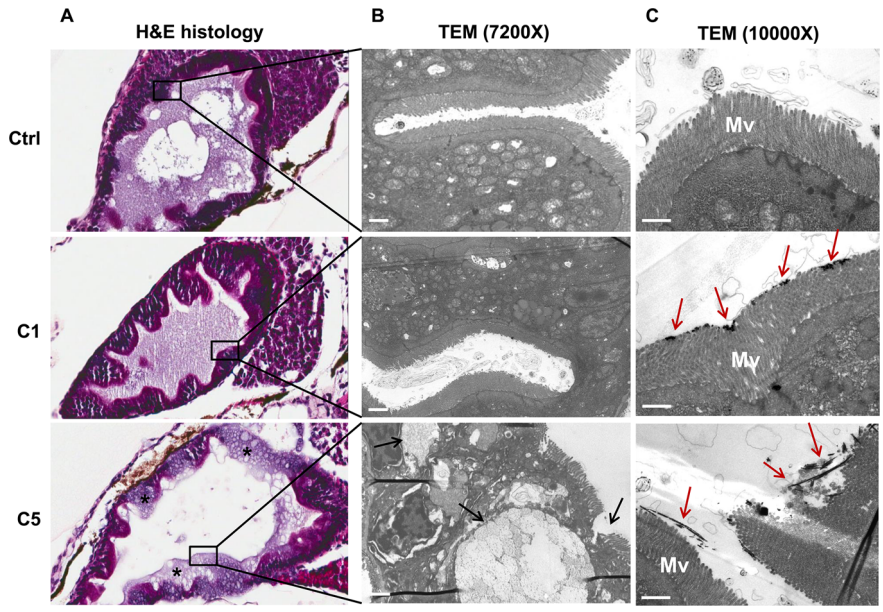

Figure 8. Histological and TEM analysis of the GIT. (A) Histopathology analysis shows the structural damage by C5 (but not C1) to the GIT. C5-exposed larvae showed desquamation of enterocytes and damage to the epithelial lining (marked by *). The control larvae and C1-exposed larvae showed normal enterocyte histology and an intact lining. (B) TEM analysis of a thin GIT section reveals ultrastructural damage by C5. This included blunting or loss of microvilli (marked by black arrows). (C) TEM analysis of the GIT immediately following CeO_2 exposure for 6 h. While C1 agglomerates could be seen to loosely adhere to the tips of the microvilli, C5 bundles could be seen to pierce through the microvilli, disrupting their integrity (marked by red arrows). Mv = microvilli. Scale bar: 1 μm.

demonstration of a good correlation between the pro-fibrogenic effects and *ex vivo* cellular responses for LAR CeO_2 nanorods. These findings suggest that the increased propensity toward NLRP3 inflammasome activation and IL-1β production at the cellular level is predictive of a higher likelihood of chronic lung injury.

There is a relative paucity of data for cross-species or cross-taxa comparison of the injurious effects of nanomaterials in general and for LAR materials in particular. The importance of interspecies assessment of nanoparticle toxicology was recently proposed by Stone *et al.*,[55] because there are insufficient data or a mechanistic understanding of nanomaterial hazards across taxa. As a rule, most studies are exclusively conducted in either a mammalian or an aquatic system and do not pick up the unique structure–activity relationships that we show for CeO_2 nanorods in the mouse lung *vs* the zebrafish GIT. Although the injury mechanism in the zebrafish did not appear to be associated with the same lysosomal damage as in the lung of mice, a novel mechanism showing microvillus injury emerged in the former organism. Our study is a promising step toward future SAR developments to predict the toxicity of engineered nanomaterials across different taxa.

While zebrafish larvae corroborate the importance of AR, the target is the GIT at a development stage during which the animals can ingest the C5 nanorods. In contrast, no effect is seen in larvae without a mouth or embryos (not shown) in which the pore sizes in the chorion are too small to allow particles access to the chorionic sac.[12,13] This notion is further supported by ICP-OES, showing that Ce uptake in 1-day-old embryos is only marginally higher than the threshold detection limit (Figure 6). In contrast, CeO_2 exposure after the zebrafish larvae developed a mouth organ (5 dpf)[56] leads to GIT uptake and epithelial injury. This explains why larvae exposed to C5 nanorods are stunted in growth and exhibit developmental abnormalities. Because larvae less than 14 days old do not display functional gills,[57,58] the GIT is the primary target organ for immersed particulates.[59,60] Different from the pulmonary uptake in mice, there are no differences in the retention of CeO_2 nanorods and nanospheres in the GIT of zebrafish larvae, with most of the ingested materials being cleared within 24 h (Figure 7B). This suggests that the epithelial injury by the C5 nanorods occurs during passage through the GIT rather than adsorption in the GIT. How exactly the microvilli are damaged is unclear but does not appear to involve a lysosomal mechanism as in the lung. These data showing LAR effects in zebrafish are novel and also provide a novel structure–activity relationship that differs from the lung.

Although this study was not intended to provide a direct comparison of zebrafish with human pathology, the findings in the larvae do raise the question of whether LAR nanomaterials may be involved in GIT damage in humans. This is significant from the perspective that engineered nanomaterials are increasingly being used in food as colorants, adhesives, or anticaking agents.[5,61] Thus, gastrointestinal exposure to engineered nanomaterials is increasing in frequency.[62,63]

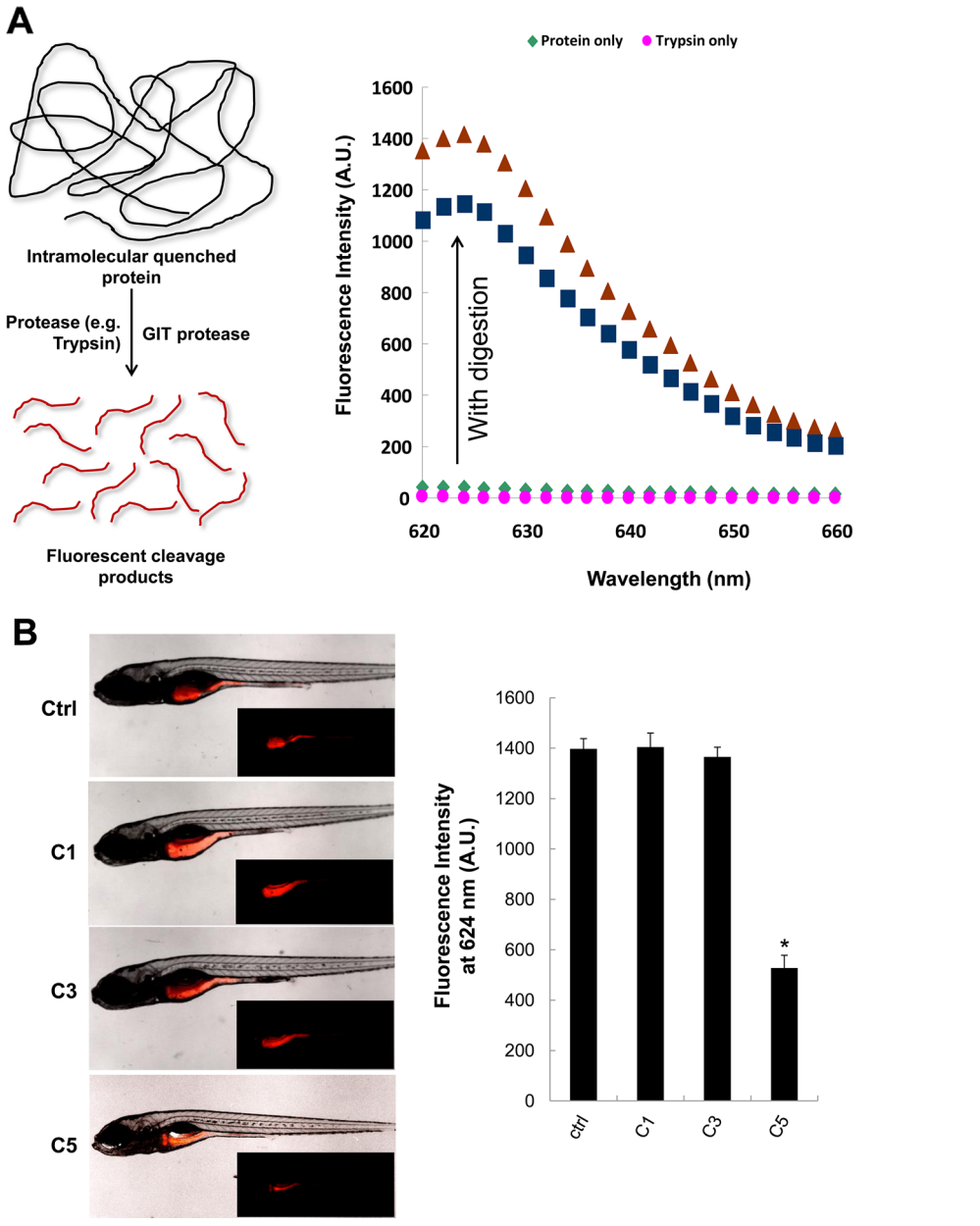

Figure 9. The digestive function of larvae exposed to C5 was significantly reduced compared to control or C1/C3-exposed larvae. (A) Explanation of the principle of digestive function testing. Quantification of the fluorescence intensity of the intramolecular-quenched protein EnzChek at 624 nm following experimental digestion by trypsin. (B) Left: Representative fluorescent images of larvae fed with EnzChek. The fluorescence intensity of the digested peptides in the GIT of larvae exposed to C5 is significantly reduced compared to the fluorescence intensity in larvae exposed to C1 and C3. Right: Average ± SD of the fluorescence intensity extracted from larvae in each group. While fluorescence intensity was significantly ($p < 0.05$) reduced for C5-exposed larvae, no decrease was seen for C1- and C3-exposed larvae.

Lomer *et al.* suggested that the average human ingests up to 10^{12} micro- or nanoparticles per day.[64] Although GIT exposure to engineered nanoparticles may not have consequences in healthy individuals, there is some preliminary evidence that people with compromised GIT function (such as Crohn's disease) might have a higher risk when exposed to particulate substances in food.[64] GIT exposure could also originate in the respiratory tract because most particulates being cleared from the lung by mucocillary transport are swallowed.[7] Oral administration of engineered nanomaterials is also increasingly being used for drug delivery and bioimaging.[65] On the basis of these observations, we will extend our studies on LAR CeO_2 to the mammalian GIT. Preliminary experiments in a human enterocyte cell line (Caco-2) have shown that C4 and C5 nanorods do induce lysosomal injury, similar to what we see in macrophages (unpublished data).

It is important to mention the limitations of our study. First, in the absence of relevant occupational or environmental exposure data, it is not possible to extrapolate our data to the dose response calculations that we could make for carbon nanotubes or Ag

nanoparticles, where some occupational exposure data were available.[26,66] We also have no idea about environmental exposure or predictive environmental concentrations of CeO_2 nanoparticles. Nonetheless, we should be able to use the platforms and methodologies developed in this study for the hazard assessment and estimating no-effect concentrations of LAR nanomaterials. Second, due to logistic limitations, the temporal analysis of CeO_2 bioavailability, onset of histological abnormalities, and development of toxicological manifestations could be performed only at limited time points. Nonetheless, the AR-dependent toxicological profiling of CeO_2 could be clearly demonstrated in both models.

CONCLUSION

We demonstrate that in addition to material composition, the AR of CeO_2 nanoparticles contribute to toxicological injury in the murine lung and the zebrafish GIT. Moreover, we demonstrate that the structure–activity analysis for CeO_2 nanorods at the subcellular level is predictive of toxicological outcome in the murine lung after correction for lung burden and dose. However, while the predictions of lysosome injury in the myeloid cells and macrophages could help to predict the generation of fibrogenic responses in the mouse lung, damage to microvilli in the GIT of zebrafish larvae does not appear to be premised on lysosomal injury.

MATERIALS AND METHODS

Materials and Reagents. The CeO_2 nanomaterials used for this study were freshly synthesized by the same hydrothermal method described previously.[6] The intramolecular-quenched protein EnzChek was purchased from Invitrogen (E6639) and was dissolved in 0.1 M sodium bicarbonate (pH 8.3) at 1 mg/mL before aliquoting and storing at −20 °C. Working stock concentrations of EnzChek (20 μg/mL) were prepared by diluting the stock solution 50× in Holtfreter's medium. Calcein was purchased from Sigma-Aldrich (C0875) and was dissolved in Holtfreter's medium at 1 mg/mL before aliquoting and storing at −20 °C. The working concentration of calcein was 20 μg/mL.

Physicochemical Characterizations of CeO_2 Library Materials. The primary diameter and length of CeO_2 nanomaterials were determined by TEM, while the suspended particles were used for assessment of hydrodynamic size and surface charge. CeO_2 nanomaterials were dispersed in deionized water by vortexing and bath sonication to yield a stock solution of 5 mg/mL as previously described.[8] The hydrodynamic sizes of the CeO_2, dispersed in deionized water, DMEM cell culture medium (supplemented with 10% FBS), and Holtfreter's medium (supplemented with 100 ug/mL alginate) were determined by high-throughput dynamic light scattering (Dynapro Plate Reader, Wyatt Technology), as described by Ji *et al.*[67] The surface charge of CeO_2 was determined by a ZetaPALS instrument (Brookhaven Instruments, Holtsville, NY, USA). The ζ-potential was derived using the Helmholtz–Smoluchowski equation based on the measurements of the electrophoretic mobility of CeO_2 in deionized water and Holtfreter's medium.

Cellular Culture and Co-incubation with CeO_2 Nanorods. THP-1 cells were suspended in RPMI 1640 medium supplemented with 10% fetal bovine serum in 75 cm^2 flasks. Before exposure to CeO_2 nanoparticles, THP-1 cells were pretreated with 1 μg/mL phorbol 12-myristate acetate overnight and primed with 10 ng/mL lipopolysaccharide (LPS). Aliquots of 3×10^4 primed cells were cultured in 0.1 mL of medium with CeO_2 nanoparticles in 96-well plates (Costar, Corning, NY, USA) at 37 °C for 24 h. All the CeO_2 nanoparticle suspensions were freshly prepared. After 24 h, the supernatants were collected for the measurement of IL-1β activity (BD Biosciences, San Diego, CA, USA) using ELISA kits according to the manufacturer's instructions. Concentrations were expressed as pg/mL.

Bone marrow-derived macrophages were differentiated in DMEM with 10% endotoxin-free fetal bovine serum and 20% M-CSF-conditioned medium for 7 days, then plated at $\sim 1.0 \times 10^6$ cells/mL and cultured for 2 days. BMDMs were primed with 500 ng/mL LPS for 5 h and then treated with the CeO_2 nanoparticles. After 24 h of culture, the supernatants were collected for the measurement of IL-1β activity using the ELISA kit described above.

Assessment of Toxicological Responses in the Mouse Lung by Oropharyngeal Aspiration. Eight-week-old male C57BL/6 mice were purchased from Charles River Laboratories (Hollister, CA, USA). All animals were housed under standard laboratory conditions established by the UCLA and NIH Guidelines for the Care and Use of Laboratory Animals in Research (DHEW78-23). Experimentation was approved by the Chancellor's Animal Research Committee at UCLA and include standard operating procedures for animal housing (filter-topped cages; room temperature at 23 ± 2 °C; 60% relative humidity; 12 h light, 12 h dark cycle) and hygiene status (autoclaved food and acidified water). Animal exposure to CeO_2 nanoparticles was carried out by oropharyngeal aspiration as described previously. Briefly, the animals were anesthetized by intraperitoneal injection of ketamine (100 mg/kg)/xylazine (10 mg/kg) in a total volume of 100 μL. With the anesthetized animals held in a vertical position, 50 μL suspensions containing the particles at 10, 20, 40, and 80 μg in PBS (equivalent to 0.5, 1.0, 2.0, and 4.0 mg/kg) were instilled at the back of the tongue to allow aspiration to the lung as described previously.[68] We used 6 animals per group. Control animals received the same volume of PBS. The positive control group in each experiment was composed of animals receiving 5.0 mg/kg quartz (Min-U-Sil). The mice were sacrificed at 40 h, 21 d, or 44 d postexposure, and BALF and lung tissues were collected. The BALF was used to perform total and differential cell counts and to measure the levels of LIX, IL-1β, and TGF-β1. Lung sections were stained with hematoxylin/eosin or with Masson's trichrome to visualize collagen deposition. LIX, IL-1β (BD Biosciences) and TGF-β1 (Promega, Madison, WI, USA) levels in the BALF were analyzed using ELISA kits according to the manufacturer's instructions. Concentrations were expressed as pg/mL.

Sircol Assay for Total Collagen Production in Lung Tissue. The right cranial lobe of each lung was suspended in PBS at ~50 mg tissue/mL and homogenized for 60 s with a tissue homogenizer (Fisher Scientific). Acetic acid was added to each sample to a final concentration of 0.5 M and incubated at 4 °C overnight. Cellular debris was removed by centrifugation, and the supernatant analyzed for total protein, using a BCA assay kit (Pierce/ThermoFisher Scientific). The Sircol-soluble collagen assay kit (Biocolor Ltd., Carrickfergus, UK) was used to extract collagen from duplicate samples using 200 μL of supernatant and 800 μL of dye reagent according to the manufacturer's instructions. Similarly prepared collagen standards (10–50 μg) were run in parallel. Collagen pellets were washed twice with denatured alcohol and dried before suspension in alkali reagent. Absorbance at 555 nm was read on a plate reader (SpectroMax M5e, Molecular Devices Corp., Sunnyvale, CA, USA). Data were expressed as μg of soluble collagen per mg of total protein.

Pulse-Exposure of Zebrafish Larvae and Assessment of Health Status. The developmental stages of zebrafish embryos and larvae were determined according to the published procedure of Kimmel *et al.*[69] For pulse exposure, groups of 30 growth-synchronized larvae at day 5 postfertilization (5 dpf) were immersed in 3 mL of 25 ug/mL CeO_2 suspensions in Petri dishes for 6 h at 28.5 °C. Following pulse exposure, the developing

larvae were carefully washed in Holtfreter's medium three times before being placed in standard aquarium tanks (3 L) for regular feeding and water circulation. The second and third pulse exposures were conducted on the same larvae at 8 and 11 dpf. Following that, the larvae were maintained in standard aquarium tanks for further observation of development and survival. In order to minimize the individual differences among larvae, larvae used in each replicate experiment were produced by the same adult breeding pair.

The overall health status of the larvae was assessed at 14 dpf based on gross morphology, body length and weight, and number of calcified vertebrae. To assess morphology, larvae were anesthetized in 0.02% tricaine and embedded in low-melt agarose gel. This allowed positioning to obtain lateral views to assess morphology, body length, and fin structure. The images were captured using an optical inverted microscope (Zeiss Observer D1). For body weight measurement, larvae were anesthetized, dried with Kimwipes, and measured using a digital balance (Denver Instrument, XP-600). The larval weights for each treatment group were normalized to the control group and plotted as weight percentage. For the measurement of calcified vertebrae, larvae were immersed in a 20 ug/mL calcein solution for 30 min at 28.5 °C. After immersion, larvae were washed three times in Holtfreter's medium to remove nonspecific staining and then embedded in low-melt agarose gel to obtain lateral views. The numbers of calcified vertebrates were counted based on the fluorescent images captured under a fluorescence microscope equipped with a 495/515 nm filter set (Zeiss Observer D1). The average number of calcified vertebrae from 10 randomly selected larvae was compared to control and AgNP- and CeO_2-exposed groups.

Confocal Raman Microscopy Analysis. Confocal Raman microscopy was performed using a Renishaw InVia model with a 514.5 nm argon laser. The laser power and beam size were ~2.5 mW and 1 μm, respectively. The Raman spectra were collected from 0 to 2000 cm^{-1} for all sample characterizations. For spectra collection, CeO_2 suspensions were dropped directly onto a glass coverslip before drying. For scanning, larvae were anesthetized and placed on a glass slide with concavity wells. The lateral view was desired for capturing full-length GIT images. Line scanning to collect Raman scattering signals was achieved by programming the motorized sample stage to move 1 μm in either the *x*- or *y*-axis direction stepwise.

ICP-OES Analysis to Determine Ce Content in the Mouse Lung and Zebrafish Larvae. The total Ce content of the lungs of mice exposed for 44 days was collected and rinsed three times with PBS. Subsequently, the lung tissues were homogenized for 60 s with a tissue homogenizer (Fisher Scientific). The probe was washed with 500 μL of PBS, which was added to the homogenate. All the homogenates were transferred to Teflon containers and acidified with 5 mL of 100% ultrahigh-purity nitric acid and digested at 95 °C for 3 h before drying and redissolving in 5% nitric acid. After digestion, the elemental Ce concentration in each sample was determined by a Shimadzu ICP-OES based on a calibration curve established by a series of concentrations of Ce standard solution (0.01−10 ppm) and expressed as μg of Ce/mg of cellular protein.

ICP-OES analysis was performed on zebrafish embryos and larvae exposed to 25 μg/mL C1 and C5 for 6 h at developmental stages 24, 72, and 120 hpf as well as 24 h after exposure in the 120 hpf group. Each exposure group included 50 embryos or larvae, which were thoroughly washed three times in Holtfreter's medium before subjecting to acid digestion as discussed above. The elemental Ce concentrations (weight/volume) were measured and expressed as μg of Ce/g of fish body weight. Groups of embryos and larvae without exposure to CeO_2 were anesthetized and weighed using a digital balance (Denver Instrument, XP-600) for calculating the fish body weight. To achieve reliable statistical analysis, three replicates were used for each group.

TEM Analysis of the GIT of Exposed Zebrafish Larvae. TEM analysis of the GIT was conducted on 5 dpf larvae, immediately after the first CeO_2 exposures (for 6 h) as well as 14 dpf (*i.e.*, 3 days after the third CeO_2 exposure). The larvae were euthanized in tricaine, and the GIT was microdissected before immersion in a 0.1 M cacodylate buffer (that includes 2% glutaraldehyde and 2% paraformaldehyde at pH 7.4), for 2 h at room temperature and then 4 °C overnight. The samples were subsequently washed in 0.1 M PBS buffer and postfixed in a solution containing 1% OsO_4 for 2 h at room temperature. After dehydration in graded ethanol (50%, 75%, 95%, 100%, 100%, 100%), the tissue samples were infiltrated in mixtures of Epon 812 and ethanol (1:1 and 2:1 ratios) for 2 h each. The tissue samples were then incubated in pure Epon 812 overnight, embedded, and cured at 60 °C for 48 h. Sections of 55−65 nm thickness (gray interference color) were cut on an ultramicrotome (RMC MTX) that utilizes a diamond knife. The sections were deposited on single-hole copper grids coated with Formvar and double-stained with an 8% uranyl acetate solution at 60 °C for 25 min, as well as lead citrate for 3 min at room temperature. Thin sections were subsequently examined with a 100CX JEOL electron microscope in the Electron Microscopy Services Center of the UCLA Brain Research Institute.

Histological Analysis of Zebrafish Larvae. Histological analysis was conducted on the developing larvae at 14 dpf. Larvae were euthanized in tricaine and fixed in 4% paraformaldehyde, first for 1 h at room temperature and then overnight at 4 °C. After fixation, the larvae were embedded in histological gel and positioned in the lateral orientation view. The samples were further processed for resin embedding, sagittal sectioning, and hematoxylin and eosin (H&E) staining in the Pathology and Laboratory Medicine Department. High-resolution images (both 20× and 40×) of the histological sections were obtained using an automated scanning system (scanning Aperio ScanScope AT).

Assessment of Digestive Function in the Zebrafish Gut. Larvae at 6 dpf (24 h after first exposure) were immersed in the EnzChek solution at 20 μg/mL for 2 h at 28.5 °C. The larvae were gently washed three times in Holtfreter's medium, anesthetized, and positioned in lateral view orientation in low-melt agarose gel on a glass-bottom dish. The fluorescence images were captured by a fluorescence microscope (Zeiss Observer D1) with a 575/620 nm filter set. The images were further analyzed by ImageJ software (NIH).

Zebrafish Husbandry. Wild-type adult zebrafish (*Danio rerio*, AB strain) were housed and maintained in the UCLA zebrafish facility on a 14L:10D photoperiod. Two pairs of male/female fish were placed in a single cage a day ahead of time and released the next morning to trigger spawning. The embryos were collected at 2 hpf and rinsed with Holtfreter's solution to remove any residue on the chorion. The embryos were subsequently examined under a stereomicroscope (Zeiss, Stemi 2000) for viability and developmental stage before being subjected to embryo screening and larvae experiments. All procedures were carried out in accordance with the Animal Care and Use Committee guidelines at UCLA.

Statistical Methods. Results were statistically analyzed using two-side Student's *t* test. The difference is regarded statistically significant if the *p* value is less than 0.05. Data are reported as the mean ± standard deviation from at least three separate experiments.

Conflict of Interest: The authors declare no competing financial interest.

Acknowledgment. The studies on the mouse lung and the development of the CeO_2 nanoparticle library were primarily supported by U19 ES019528 and RO1 ES016746. The studies on the zebrafish larvae were supported by UC CEIN funding from the National Science Foundation and the Environmental Protection Agency under Cooperative Agreement Number DBI 1266377. Any opinions, findings, and conclusions or recommendations expressed in this material are those of the author(s) and do not necessarily reflect the views of the National Science Foundation or the Environmental Protection Agency. This work has not been subjected to EPA review, and no official endorsement should be inferred.

Supporting Information Available: Additional figures on the IL-1β production by THP1 and bone marrow derived macrophages after exposure to CeO_2 nanoparticles, H&E-stained lung section from mice exposed to CeO_2 for 40 h, Masson's

trichrome-stained lung section from mice exposed to CeO_2 for 21 days, representative microscopic images of zebrafish larvae in control and CeO_2-exposed groups, representative TEM images of the pseudofeces containing CeO_2 nanospheres (C1) and nanorods (C5), and representative TEM images showing the interaction of C5 with microvilli in the gastrointestinal tract of zebrafish larvae. This material is available free of charge *via* the Internet at http://pubs.acs.org.

REFERENCES AND NOTES

1. Huynh, W. U.; Dittmer, J. J.; Alivisatos, A. P. Hybrid Nanorod-Polymer Solar Cells. *Science* **2002**, *295*, 2425–2427.
2. Jana, N. R.; Gearheart, L.; Murphy, C. J. Wet Chemical Synthesis of High Aspect Ratio Cylindrical Gold Nanorods. *J. Phys. Chem. B* **2001**, *105*, 4062–4067.
3. Murphy, C. J.; Jana, N. R. Controlling the Aspect Ratio of Inorganic Nanorods and Nanowires. *Adv. Mater.* **2002**, *14*, 80–82.
4. Nakayama, K.; Kubo, T.; Nishikitani, Y. Anodic Formation of Titania Nanotubes with Ultrahigh Aspect Ratio. *Electrochem. Solid State* **2008**, *11*, C23–C26.
5. Duncan, T. V. Applications of Nanotechnology in Food Packaging and Food Safety: Barrier Materials, Antimicrobials and Sensors. *J. Colloid Interface Sci.* **2011**, *363*, 1–24.
6. Ji, Z.; Wang, X.; Zhang, H.; Lin, S.; Meng, H.; Sun, B.; George, S.; Xia, T.; Nel, A. E.; Zink, J. I. Designed Synthesis of CeO_2 Nanorods and Nanowires for Studying Toxicological Effects of High Aspect Ratio Nanomaterials. *ACS Nano* **2012**, *6*, 5366–5380.
7. Cassee, F. R.; van Balen, E. C.; Singh, C.; Green, D.; Muijser, H.; Weinstein, J.; Dreher, K. Exposure, Health and Ecological Effects Review of Engineered Nanoscale Cerium and Cerium Oxide Associated with Its Use as a Fuel Additive. *Cr. Rev. Toxicol.* **2011**, *41*, 213–229.
8. Zhang, J.; Ju, X.; Wu, Z. J.; Liu, T.; Hu, D.; Xie, Y. N. Structural Characteristics of Cerium Oxide Nanocrystals Prepared by the Microemulsion Method. *Chem. Mater.* **2001**, *13*, 4192–4197.
9. Mai, H. X.; Sun, L. D.; Zhang, Y. W.; Si, R.; Feng, W.; Zhang, H. P.; Liu, H. C.; Yan, C. H. Shape-Selective Synthesis and Oxygen Storage Behavior of Ceria Nanopolyhedra, Nanorods, and Nanocubes. *J. Phys. Chem. B* **2005**, *109*, 24380–24385.
10. Zhou, K.; Yang, Z.; Yang, S. Highly Reducible CeO_2 Nanotubes. *Chem. Mater.* **2007**, *19*, 1215–1217.
11. Ma, J. Y.; Mercer, R. R.; Barger, M.; Schwegler-Berry, D.; Scabilloni, J.; Ma, J. K.; Castranova, V. Induction of Pulmonary Fibrosis by Cerium Oxide Nanoparticles. *Toxicol. Appl. Pharmacol.* **2012**, *262*, 255–264.
12. Lin, S.; Zhao, Y.; Xia, T.; Meng, H.; Ji, Z.; Liu, R.; George, S.; Xiong, S.; Wang, X.; Zhang, H.; *et al*. High Content Screening in Zebrafish Speeds up Hazard Ranking of Transition Metal Oxide Nanoparticles. *ACS Nano* **2011**, *5*, 7284–7295.
13. Lin, S.; Zhao, Y.; Ji, Z.; Ear, J.; Chang, C. H.; Zhang, H.; Low-Kam, C.; Yamada, K.; Meng, H.; Wang, X.; *et al*. Zebrafish High-Throughput Screening to Study the Impact of Dissolvable Metal Oxide Nanoparticles on the Hatching Enzyme, ZHE1. *Small* **2013**, *9*, 1776–1785.
14. Lin, S.; Zhao, Y.; Nel, A. E.; Lin, S. Zebrafish: An *in Vivo* Model for Nano EHS Studies. *Small* **2012**, *9*, 1608–1618.
15. Meng, H.; Xia, T.; George, S.; Nel, A. E. A Predictive Toxicological Paradigm for the Safety Assessment of Nanomaterials. *ACS Nano* **2009**, *3*, 1620–1627.
16. Bonner, J. C.; Silva, R. M.; Taylor, A. J.; Brown, J. M.; Hilderbrand, S. C.; Castranova, V.; Porter, D.; Elder, A.; Oberdorster, G.; Harkema, J. R.; *et al*. Interlaboratory Evaluation of Rodent Pulmonary Responses to Engineered Nanomaterials: The NIEHS Nano Go Consortium. *Environ. Health Persp.* **2013**, *121*, 676–682.
17. Nel, A. E.; Xia, T.; Meng, H.; Wang, X.; Lin, S.; Ji, Z.; Zhang, H. Nanomaterials Toxicity Testing in the 21st Century: Use of a Predictive Toxicological Approach and High-Throughput Screening. *Acc. Chem. Res.* **2012**, *46*, 607–621.
18. Hamilton, R. F.; Wu, N.; Porter, D.; Buford, M.; Wolfarth, M.; Holian, A. Particle Length-Dependent Titanium Dioxide Nanomaterials Toxicity and Bioactivity. *Part. Fibre Toxicol.* **2009**, *6*, 35.
19. Porter, D. W.; Wu, N.; Hubbs, A. F.; Mercer, R. R.; Funk, K.; Meng, F.; Li, J.; Wolfarth, M. G.; Battelli, L.; Friend, S.; *et al*. Differential Mouse Pulmonary Dose and Time Course Responses to Titanium Dioxide Nanospheres and Nanobelts. *Toxicol. Sci.* **2013**, *131*, 179–193.
20. Donaldson, K.; Murphy, F.; Schinwald, A.; Duffin, R.; Poland, C. A. Identifying the Pulmonary Hazard of High Aspect Ratio Nanoparticles to Enable Their Safety-by-Design. *Nanomedicine* **2011**, *6*, 143–156.
21. Tomatis, M.; Turci, F.; Ceschino, R.; Riganti, C.; Gazzano, E.; Martra, G.; Ghigo, D.; Fubini, B. High Aspect Ratio Materials: Role of Surface Chemistry *vs*. Length in the Historical "Long and Short Amosite Asbestos Fibers". *Inhal. Toxicol.* **2010**, *22*, 984–998.
22. Oberdörster, G.; Stone, V.; Donaldson, K. Toxicology of Nanoparticles: A Historical Perspective. *Nanotoxicology* **2007**, *1*, 2–25.
23. Blake, T.; Castranova, V.; Schwegler-Berry, D.; Baron, P.; Deye, G. J.; Li, C. H.; Jones, W. Effect of Fiber Length on Glass Microfiber Cytotoxicity. *J. Toxicol. Env. Heal. A* **1998**, *54*, 243–259.
24. Li, R. B.; Wang, X.; Ji, Z. X.; Sun, B. B.; Zhang, H. Y.; Chang, C. H.; Lin, S. J.; Meng, H.; Liao, Y. P.; Wang, M. Y.; *et al*. Surface Charge and Cellular Processing of Covalently Functionalized Multiwall Carbon Nanotubes Determine Pulmonary Toxicity. *ACS Nano* **2013**, *7*, 2352–2368.
25. Wang, X.; Xia, T.; Duch, M. C.; Ji, Z. X.; Zhang, H. Y.; Li, R. B.; Sun, B. B.; Lin, S. J.; Meng, H.; Liao, Y. P.; *et al*. Pluronic F108 Coating Decreases the Lung Fibrosis Potential of Multiwall Carbon Nanotubes by Reducing Lysosomal Injury. *Nano Lett.* **2012**, *12*, 3050–3061.
26. Wang, X.; Xia, T.; Ntim, S. A.; Ji, Z. X.; Lin, S. J.; Meng, H.; Chung, C. H.; George, S.; Zhang, H. Y.; Wang, M. Y.; *et al*. Dispersal State of Multiwalled Carbon Nanotubes Elicits Profibrogenic Cellular Responses That Correlate with Fibrogenesis Biomarkers and Fibrosis in the Murine Lung. *ACS Nano* **2011**, *5*, 9772–9787.
27. Rodea-Palomares, I.; Boltes, K.; Fernandez-Pinas, F.; Leganes, F.; Garcia-Calvo, E.; Santiago, J.; Rosal, R. Physicochemical Characterization and Ecotoxicological Assessment of CeO_2 Nanoparticles Using Two Aquatic Microorganisms. *Toxicol. Sci.* **2011**, *119*, 135–145.
28. Manier, N.; Garaud, M.; Delalain, P.; Aguerre-Chariol, O.; Pandard, P. Behaviour of Ceria Nanoparticles in Standardized Test Media – Influence on the Results of Ecotoxicological Tests. *J. Phys. (Paris)* **2011**, *304*, 012058.
29. Roberts, A. P.; Mount, A. S.; Seda, B.; Souther, J.; Qiao, R.; Lin, S.; Ke, P. C.; Rao, A. M.; Klaine, S. J. *In Vivo* Biomodification of Lipid-Coated Carbon Nanotubes by *Daphnia magna*. *Environ. Sci. Technol.* **2007**, *41*, 3025–3029.
30. Cheng, J.; Chan, C. M.; Veca, L. M.; Poon, W. L.; Chan, P. K.; Qu, L.; Sun, Y. P.; Cheng, S. H. Acute and Long-Term Effects after Single Loading of Functionalized Multi-Walled Carbon Nanotubes into Zebrafish (*Danio rerio*). *Toxicol. Appl. Pharmacol.* **2009**, *235*, 216–225.
31. Smith, C. J.; Shaw, B. J.; Handy, R. D. Toxicity of Single Walled Carbon Nanotubes to Rainbow Trout, (*Oncorhynchus mykiss*): Respiratory Toxicity, Organ Pathologies, and Other Physiological Effects. *Aquat. Toxicol.* **2007**, *82*, 94–109.
32. Fraser, T. W.; Reinardy, H. C.; Shaw, B. J.; Henry, T. B.; Handy, R. D. Dietary Toxicity of Single-Walled Carbon Nanotubes and Fullerenes (C_{60}) in Rainbow Trout (*Oncorhynchus mykiss*). *Nanotoxicology* **2011**, *5*, 98–108.
33. Ispas, C.; Andreescu, D.; Patel, A.; Goia, D. V.; Andreescu, S.; Wallace, K. N. Toxicity and Developmental Defects of Different Sizes and Shape Nickel Nanoparticles in Zebrafish. *Environ. Sci. Technol.* **2009**, *43*, 6349–6356.
34. Scanlan, L.; Reed, R. B.; Loguinov, A. V.; Antczak, P.; Tagmount, A.; Aloni, S.; Nowinski, D. T.; Luong, P.; Tran, C.; Karunaratne, N.; *et al*. Silver Nanowire Exposure Results in Internalization and Toxicity to *Daphnia magna*. *ACS Nano* **2013**, *7*, 10681–10694.

35. Asharani, P. V.; Lian, W. Y.; Gong, Z.; Valiyaveettil, S. Toxicity of Silver Nanoparticles in Zebrafish Models. *Nanotechnology* **2008**, *19*, 255102.
36. Powers, C. M.; Yen, J.; Linney, E. A.; Seidler, F. J.; Slotkin, T. A. Silver Exposure in Developing Zebrafish (*Danio rerio*): Persistent Effects on Larval Behavior and Survival. *Neurotoxicol. Teratol.* **2010**, *32*, 391–397.
37. George, S.; Lin, S.; Ji, Z.; Thomas, C. R.; Li, L.; Mecklenburg, M.; Meng, H.; Wang, X.; Zhang, H.; Xia, T.; *et al*. Surface Defects on Plate-Shaped Silver Nanoparticles Contribute to Its Hazard Potential in a Fish Gill Cell Line and Zebrafish Embryos. *ACS Nano* **2012**, *6*, 3745–3759.
38. Du, S. J.; Frenkel, V.; Kindschi, G.; Zohar, Y. Visualizing Normal and Defective Bone Development in Zebrafish Embryos Using the Fluorescent Chromophore Calcein. *Dev. Biol.* **2001**, *238*, 239–246.
39. Rekhi, S.; Saxena, S. K.; Lazor, P. High-Pressure Raman Study on Nanocrystalline CeO_2. *J. Appl. Phys.* **2001**, *89*, 2968–2971.
40. Spanier, J.; Robinson, R.; Zhang, F.; Chan, S.-W.; Herman, I. Size-Dependent Properties of CeO_2-Y Nanoparticles as Studied by Raman Scattering. *Phys. Rev. B* **2001**, *64*, 245407.
41. Hama, K.; Provost, E.; Baranowski, T. C.; Rubinstein, A. L.; Anderson, J. L.; Leach, S. D.; Farber, S. A. *In Vivo* Imaging of Zebrafish Digestive Organ Function Using Multiple Quenched Fluorescent Reporters. *Am. J. Physiol. Gastrointest. Liver Physiol.* **2009**, *296*, G445–G453.
42. Otis, J. P.; Farber, S. A. Imaging Vertebrate Digestive Function and Lipid Metabolism *in Vivo*. *Drug Discovery Today* **2012**, *10*, e11–e16.
43. HEI - Health Effects Institute, R. R., **2001**. *Evaluation of Human Health Risk from Cerium Added to Diesel Fuel*, HEI Research Communication 9; Flagship Press: North Andover, MA, http://pubs.healtheffects.org/view.php?id = 172.
44. Waring, P. M.; Watling, R. J. Rare-Earth Deposits in a Deceased Movie Projectionist - a New Case of Rare-Earth Pneumoconiosis. *Med. J. Australia* **1990**, *153*, 726–730.
45. Mcdonald, J. W.; Ghio, A. J.; Sheehan, C. E.; Bernhardt, P. F.; Roggli, V. L. Rare-Earth (Cerium Oxide) Pneumoconiosis - Analytical Scanning Electron-Microscopy and Literature-Review. *Mod. Pathol.* **1995**, *8*, 859–865.
46. Eom, H. J.; Choi, J. Oxidative Stress of CeO_2 Nanoparticles Via P38-Nrf-2 Signaling Pathway in Human Bronchial Epithelial Cell, Beas-2B. *Toxicol. Lett.* **2009**, *187*, 77–83.
47. Yokel, R. A.; Florence, R. L.; Unrine, J. M.; Tseng, M. T.; Graham, U. M.; Wu, P.; Grulke, E. A.; Sultana, R.; Hardas, S. S.; Butterfield, D. A. Biodistribution and Oxidative Stress Effects of a Systemically-Introduced Commercial Ceria Engineered Nanomaterial. *Nanotoxicology* **2009**, *3*, 234–248.
48. Zhang, H.; Ji, Z.; Xia, T.; Meng, H.; Low-Kam, C.; Liu, R.; Pokhrel, S.; Lin, S.; Wang, X.; Liao, Y. P.; *et al*. Use of Metal Oxide Nanoparticle Band Gap to Develop a Predictive Paradigm for Oxidative Stress and Acute Pulmonary Inflammation. *ACS Nano* **2012**, *6*, 4349–4368.
49. Das, M.; Patil, S.; Bhargava, N.; Kang, J. F.; Riedel, L. M.; Seal, S.; Hickman, J. J. Auto-Catalytic Ceria Nanoparticles Offer Neuroprotection to Adult Rat Spinal Cord Neurons. *Biomaterials* **2007**, *28*, 1918–1925.
50. Perez, J. M.; Asati, A.; Nath, S.; Kaittanis, C. Synthesis of Biocompatible Dextran-Coated Nanoceria with pH-Dependent Antioxidant Properties. *Small* **2008**, *4*, 552–556.
51. Li, R.; Ji, Z.; Chang, C. H.; Dunphy, D. R.; Cai, X.; Meng, H.; Zhang, H.; Sun, B.; Wang, X.; Dong, J.; *et al*. Surface Interactions with Compartmentalized Cellular Phosphates Explain Rare Earth Oxide Nanoparticle Hazard and Provide Opportunities for Safer Design. *ACS Nano* **2014**, *8*, 1771–1783.
52. Bonner, J. C. Mesenchymal Cell Survival in Airway and Interstitial Pulmonary Fibrosis. *Fibrog. Tissue Repair* **2010**, *3*, 15.
53. Mcclure, J.; Cameron, C. H. S.; Garrett, R. The Ultrastructural Features of Malakoplakia. *J. Pathol.* **1981**, *134*, 13–25.
54. Donaldson, K.; Murphy, F. A.; Duffin, R.; Poland, C. A. Asbestos, Carbon Nanotubes and the Pleural Mesothelium: A Review of the Hypothesis Regarding the Role of Long Fibre Retention in the Parietal Pleura, Inflammation and Mesothelioma. *Part. Fibre Toxicol.* **2010**, *7*, 5.
55. Gaiser, B. K.; Fernandes, T. F.; Jepson, M. A.; Lead, J. R.; Tyler, C. R.; Baalousha, M.; Biswas, A.; Britton, G. J.; Cole, P. A.; Johnston, B. D.; *et al*. Interspecies Comparisons on the Uptake and Toxicity of Silver and Cerium Dioxide Nanoparticles. *Environ. Toxicol. Chem.* **2012**, *31*, 144–154.
56. Ng, A. N.; de Jong-Curtain, T. A.; Mawdsley, D. J.; White, S. J.; Shin, J.; Appel, B.; Dong, P. D.; Stainier, D. Y.; Heath, J. K. Formation of the Digestive System in Zebrafish: III. Intestinal Epithelium Morphogenesis. *Dev. Biol.* **2005**, *286*, 114–135.
57. Rombough, P. Gills Are Needed for Ionoregulation before They Are Needed for O_2 Uptake in Developing Zebrafish, Danio Rerio. *J. Exp. Biol.* **2002**, *205*, 1787–1794.
58. McLeish, J. A.; Chico, T. J.; Taylor, H. B.; Tucker, C.; Donaldson, K.; Brown, S. B. Skin Exposure to Micro- and Nano-Particles Can Cause Haemostasis in Zebrafish Larvae. *Thromb. Haemostasis* **2010**, *103*, 797–807.
59. Farkas, J.; Christian, P.; Urrea, J. A.; Roos, N.; Hassellov, M.; Tollefsen, K. E.; Thomas, K. V. Effects of Silver and Gold Nanoparticles on Rainbow Trout (*Oncorhynchus mykiss*) Hepatocytes. *Aquat. Toxicol.* **2010**, *96*, 44–52.
60. Griffitt, R. J.; Brown-Peterson, N. J.; Savin, D. A.; Manning, C. S.; Boube, I.; Ryan, R. A.; Brouwer, M. Effects of Chronic Nanoparticulate Silver Exposure to Adult and Juvenile Sheepshead Minnows (*Cyprinodon variegatus*). *Environ. Toxicol. Chem.* **2012**, *31*, 160–167.
61. Chaudhry, Q.; Scotter, M.; Blackburn, J.; Ross, B.; Boxall, A.; Castle, L.; Aitken, R.; Watkins, R. Applications and Implications of Nanotechnologies for the Food Sector. *Food Addit. Contam. A* **2008**, *25*, 241–258.
62. Hoet, P. H.; Bruske-Hohlfeld, I.; Salata, O. V. Nanoparticles - Known and Unknown Health Risks. *J. Nanobiotechnol.* **2004**, *2*, 12.
63. Powell, J. J.; Faria, N.; Thomas-McKay, E.; Pele, L. C. Origin and Fate of Dietary Nanoparticles and Microparticles in the Gastrointestinal Tract. *J. Autoimmun.* **2010**, *34*, J226–J233.
64. Lomer, M. C. E.; Thompson, R. P. H.; Powell, J. J. Fine and Ultrafine Particles of the Diet: Influence on the Mucosal Immune Response and Association with Crohn's Disease. *Proc. Nutr. Soc.* **2007**, *61*, 123–130.
65. Uskokovic, V.; Lee, K.; Lee, P. P.; Fischer, K. E.; Desai, T. A. Shape Effect in the Design of Nanowire-Coated Microparticles as Transepithelial Drug Delivery Devices. *ACS Nano* **2012**, *6*, 7832–7841.
66. Wang, X.; Ji, Z.; Chang, C. H.; Zhang, H.; Wang, M.; Liao, Y. P.; Lin, S.; Meng, H.; Li, R.; Sun, B.; *et al*. Use of Coated Silver Nanoparticles to Understand the Relationship of Particle Dissolution and Bioavailability to Cell and Lung Toxicological Potential. *Small* **2013**, *10*, 385–398.
67. Ji, Z.; Jin, X.; George, S.; Xia, T.; Meng, H.; Wang, X.; Suarez, E.; Zhang, H.; Hoek, E. M. V.; Godwin, H.; *et al*. Dispersion and Stability Optimization of TiO_2 Nanoparticles in Cell Culture Media. *Environ. Sci. Technol.* **2010**, *44*, 7309–7314.
68. Li, N.; Wang, M.; Bramble, L. A.; Schmitz, D. A.; Schauer, J. J.; Sioutas, C.; Harkema, J. R.; Nel, A. E. The Adjuvant Effect of Ambient Particulate Matter Is Closely Reflected by the Particulate Oxidant Potential. *Environ. Health Persp.* **2009**, *117*, 1116–1123.
69. Kimmel, C. B.; Ballard, W. W.; Kimmel, S. R.; Ullmann, B.; Schilling, T. F. Stages of Embryonic Development of the Zebrafish. *Dev. Dyn.* **1995**, *203*, 253–310.